

### Diffusive motion on a fractal; $G_{nm}(t)$

R. A. Guyer

Schlumberger-Doll Research, Old Quarry Road, Ridgefield, Connecticut 06877

(Received 13 June 1984; revised manuscript received 27 June 1985)

The conditional probability that a particle at site  $m$  at time 0 will be at site  $n$  at time  $t$  is studied numerically and analytically on the Sierpiński gasket. The Laplace transform of  $G_{nm}(t)$ ,  $G_{nm}(s)$ , is found to behave on average as  $\exp(-|n-m|s^{1/d_w})$  for large  $|n-m|s^{1/d_w}$ . Fluctuations about this average behavior are found to be mild when the distance between sites  $m$  and  $n$  is taken to be the "lacunar" distance. Analytic arguments for the asymptotic behavior of  $G_{nm}(s)$ , based on the scaling of coupling constants under renormalization, are made.  $G_{nm}(t)$  is found to have the asymptotic behavior  $\exp[-(|n-m|/t^{1/d_w})^\nu]$ ,  $\nu=d_w(d_w-1)^{-1}$  in agreement with a result of Fisher [J. Chem. Phys. **44**, 616 (1966)]. The relationship of this form of  $G_{nm}(t)$  to that proposed by Banavar and Willemsen is clarified.

#### I. INTRODUCTION

There is currently considerable interest in studies of the geometry of fractally structured media and of the kinematics of particle motion in these media. Mandelbrot describes the geometry of fractals in his elegant book, *The Fractal Geometry of Nature*.<sup>1</sup> Particle motion on a fractal, as simple as that of a random walker, requires clarification of the basic concepts employed in a kinematic description.<sup>2,3</sup> The geometry of a fractal is characterized by the "fractal (Hausdorff) dimension,"  $d_F$ . Particle kinematics, for a random walker, is characterized by the "dimension of the walk,"  $d_w$ . The "spectral dimension,"  $d_s$ , defined in terms of the  $\omega \rightarrow 0$  density of states involves both geometry and kinematics. A great deal is known about the average properties of geometry and kinematics in the form of scaling relations that involve  $d_F$ ,  $d_w$ ,  $d_s$ , and others.<sup>2,3,4</sup>

(1) If the resistance scales with length as  $R(L) \sim L^r$  and if the conductivity scales with length as  $\sigma(L) \sim L^{-\tilde{r}}$ , then in  $d$  dimensions<sup>5</sup>

$$d - 2 + r = \tilde{r}. \tag{1}$$

(2) For particle motion with  $\langle x^2 \rangle \cong (Wt)^{2/d_w}$  ( $W$  is the coupling constant in the diffusion equation), if the coupling constant scales with length as  $W(L) \sim L^{-w}$ , then<sup>6</sup>

$$d_F - 2 + w = \tilde{\delta}, \tag{2}$$

where  $d_w = 2 + \tilde{\delta}$ .

(3) Equations (1) and (2) lead to the Einstein relation<sup>6,7</sup>

$$\tilde{\delta} = d_F - d - \tilde{r}, \tag{3}$$

or  $D(L) \cong n(L)\sigma(L)$ , since  $w=r$ . Here  $D(L)$ ,  $n(L)$ , and  $\sigma(L)$  are the diffusion constant, density, and conductivity, respectively.

(4) The spectral dimension is equal to  $\frac{4}{3}$  on a Cayley tree<sup>8</sup> and on structures of the type described by Rammal and Toulouse.<sup>3,8</sup> It is near  $\frac{4}{3}$  on percolation clusters near threshold. The literature that addresses the Alexander-Orbach conjecture (i.e.,  $d_s = \frac{4}{3}$ ) is substantial and of in-

terest to physics and sociology.

The purpose of this paper is to describe a study of  $G_{nm}(t)$ , the conditional probability, the probability that a particle at site  $m$  at time 0 will be at site  $n$  at time  $t$ , for a random walker on a fractal. This conditional probability contains some of the average information that is in the scaling relations; e.g.,

$$\langle x^2 \rangle = \int d\mathbf{x}' |\mathbf{x} - \mathbf{x}'|^2 G(\mathbf{x}, t | \mathbf{x}', 0) \propto (Wt)^{2/d_w}. \tag{4}$$

It contains, in addition, features that are a consequence of details of the geometry of the medium through which the particle is propagating. For example, a fractally structured medium is not translationally invariant. As a consequence we do not trivially expect  $G(\mathbf{x}, t | \mathbf{x}', 0)$  to be a function only of  $|\mathbf{x} - \mathbf{x}'|$ . The dilatation invariance of a fractal means that if there are gaps on scale  $l$  of size  $\alpha l$ , then on scale  $L$  there are gaps of size  $\alpha L$ . We might expect this feature of a structure to make itself known in  $G(\mathbf{x}, t | \mathbf{x}', 0)$ , since a particle traversing distance  $l$  must skirt a gap of size  $\alpha l$ , etc.

Our study of  $G_{nm}(t)$  involves both numerical results from calculations on a Sierpiński gasket and analytic results that are in part based on these. It is organized as follows. In Sec. II we review the length-scale-renormalization (LSR) procedure for solving the diffusion equation. We describe application of this procedure to the question, "if at time zero, . . . ?," whose answer is the conditional probability we seek. A one-dimensional example is described to call attention to behavior we want to understand before tackling the less familiar case of a Sierpiński gasket. Calculations of  $G_{nm}(t)$  for a Sierpiński gasket are described in detail. In Sec. III we summarize our numerical findings and discuss the analytic behavior of  $G_{nm}(t)$ . Attention is given to constructing a scaling form for  $G$ , to the effect of lacunarity, to the consequences of the Chapman-Kolmogorov equation, etc. We make comparison with the results of Fisher<sup>10</sup> and the recent work of Banavar and Willemsen<sup>11</sup> and attempt to understand the relationship of our results to theirs.

Before we go on there is an important point that we

wish to emphasize early and to which we will in various ways call attention. We ask about  $x$  at time  $t$ . We have in mind a fixed time scale. In using the LSR procedure we examine the system on different length scales at fixed time scale. Time scale and length scale are related on average by the kinematics, e.g.,  $x^2 \cong Dt$ . There are very important properties of the physics and of the numerical and analytic procedures that depend upon the relationship between time scale and length scale. For example, examining equations on a length scale large compared to that on average associated with the time scale can have computational advantage. Comparison of expectations, calculation, etc., will make sense only if the time-scale and length-scale regimes coincide, etc.

## II. APPLICATIONS OF THE LSR PROCEDURE TO $G_{nm}(t)$ .

The length-scale-renormalization procedure, LSR procedure, has been described in detail in studies of disordered one-dimensional random walks,<sup>12</sup> of the uniform Sierpiński gaskets,<sup>6</sup> and of the Vicsek fractals.<sup>7</sup> See also Ref. 13. Here we describe application of the procedure to solution of the diffusion equation on a Sierpiński gasket. In going over what is partially old ground we call particular attention to those features of the procedure that will help us understand the calculation of  $G_{nm}(t)$ .

Consider a random walker on a Sierpiński gasket. The conditional probability,  $G_{nm}(t)$ , obeys the equation

$$\frac{\partial}{\partial t} G_{nm}(t) = -V_n G_{nm}(t) + \sum_{\delta} W_{n,n+\delta} G_{n+\delta,m}(t), \quad (5)$$

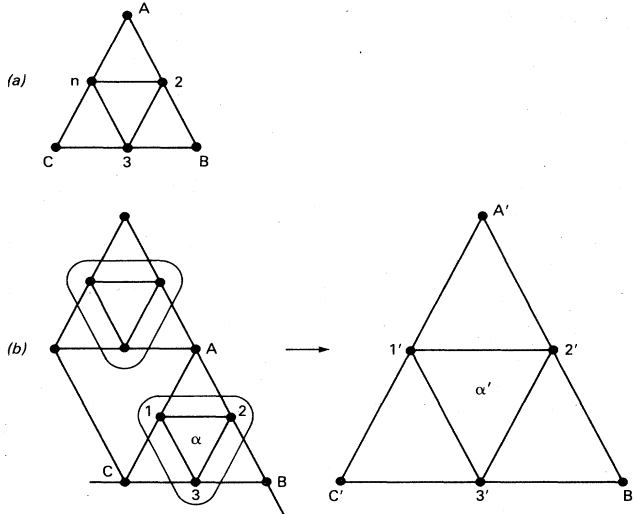


FIG. 1. The geometry of renormalization. (a) The near-neighbor sites of site  $n$  are denoted as sites  $n+\delta$  and are sites  $A$ ,  $2$ ,  $3$ , and  $C$ . (b) The renormalization procedure removes the internal sites from each plaquette, the circled sites,  $1, 2, 3$  on the left, and describes the system in terms of internal and external sites of a new plaquette;  $1', 2', 3'$  and  $A', B', C'$  on the right. The notation for plaquettes is described in the Appendix. To carry through the renormalization one must keep track of site and bond information for each plaquette.

where the sites  $\delta$  are near-neighbor sites of site  $n$  (Fig. 1),  $W_{nm} = W_{mn}$  is the rate at which a particle at site  $m$  goes to site  $n$ , and  $V_n = \sum_{\delta} W_{n+\delta,n}$ . The Laplace-transformed set of equations,

$$s\hat{G}_{nm}(s) = Z_{nm} - V_n \hat{G}_{nm}(s) + \sum_{\delta} W_{n,n+\delta} \hat{G}_{n+\delta,m}(s), \quad (6)$$

$Z_{nm} = \delta_{n,m}$ , is solved using the LSR procedure as illustrated in Fig. 1(b). The sites  $1, 2, 3$  and  $A, B, C$  are the internal and external sites, respectively, of the plaquette  $\alpha$ . The equations of motion for  $\mathbf{G}_i$  and  $\mathbf{G}_e$ , vectors that denote the set of internal and external  $G_{mn}$ 's are

$$(s\vec{I} + \vec{T}) \cdot \mathbf{G}_i = \mathbf{Z}_i + \vec{C} \cdot \mathbf{G}_e, \quad (7a)$$

$$(s\vec{I} + \vec{V}_e) \cdot \mathbf{G}_e = \mathbf{Z}_e + \vec{C}^\dagger \cdot \mathbf{G}_i, \quad (7b)$$

where the coupling between the internal sites and the external sites is given by the matrix  $\vec{C}$ ;  $\vec{T}$  and  $\vec{V}_e$  are matrices involving  $V_1, V_2, V_3$ ,  $W_{12}, W_{23}, W_{31}$  and  $V_A, V_B, V_C$  (see Table I) and  $Z_{nm} = \delta_{n,m}$ . A plaquette index on all quantities in Eqs. (7) has been suppressed as has the carat denoting the Laplace transform. Equation (7a) is solved for  $\mathbf{G}_i$  and substituted into Eq. (7b) with the result that the sites  $A, B, C$  become sites of a new plaquette  $\alpha'$  with sites  $1', 2', 3', A', B', C'$  that are coupled to one another by equations of the same form as Eq. (6) with renormalized coupling constants and with a renormalized value of the amplitudes,  $Z$ . For the new coupling constants for plaquette  $\alpha'$  we have (schematically)

$$\vec{V}' = \vec{V} - \vec{C}^\dagger \cdot \vec{D} \cdot \vec{C}, \quad (8)$$

$$\vec{C}' = \vec{C}^\dagger \cdot \vec{D} \cdot \vec{C}, \quad (9)$$

where  $\vec{V}, \vec{C}$  are appropriate to plaquette  $\alpha$ ,  $\vec{D}^{-1} = (s\vec{I} + \vec{T}_i)$ . The specific form of Eqs. (8) and (9) for a uniform gasket, in which all of the  $W_{mn}$  have the same value, is given in Ref. 6. For the renormalized value of  $Z$  we have (schematically)

$$\mathbf{Z}' = \mathbf{Z}_e + \vec{C}^\dagger \cdot \vec{D} \cdot \mathbf{Z}_i. \quad (10)$$

TABLE I. The coupling in Eq. (6) determines the matrices in Eqs. (7); the  $W$ 's are defined in Fig. 10 of the Appendix.

$$\vec{D}^{-1} = s\vec{I} + \vec{T} = \begin{bmatrix} s + V_1 & W_{12} & W_{13} \\ W_{21} & s + V_2 & W_{23} \\ W_{31} & W_{32} & s + V_3 \end{bmatrix},$$

$$W_{ij} = W_{ji};$$

$$\vec{C} = \begin{bmatrix} W_{1A} & 0 & W_{1C} \\ W_{2A} & W_{2B} & 0 \\ 0 & W_{3B} & W_{3C} \end{bmatrix},$$

$$\vec{V} = \begin{bmatrix} V_A & 0 & 0 \\ 0 & V_B & 0 \\ 0 & 0 & V_C \end{bmatrix}.$$

Solution to the diffusion equation using the LSR procedure means iteration of the recursion relations for the coupling constants. From this iteration the diagonal conditional probability can be found, i.e.,  $G_{nn}(s)$ . Examination of  $G_{nn}(s)$  establishes  $\langle x^2 \rangle \propto (Wt)^{2/d_w}$ , yields the scaling relation Eq. (2), etc. All of this can be accomplished without need to pay attention to evolution of the amplitudes under renormalization, Eq. (10). It is the evolution of the amplitudes under renormalization that contains information about the off-diagonal conditional probability,  $G_{nm}(s)$ . It is clear from Eqs. (8)–(10) that the evolution of the coupling constants under renormalization proceeds independently of the evolution of the amplitudes. The evolution of the coupling constants under renormalization has already been described in some detail. Let us turn to the evolution of the amplitudes under renormalization as given by Eq. (10).

Suppose that at  $t=0$  the particle is on internal site  $n$  plaquette  $\alpha$ . Then,  $Z_e$  is zero for all plaquettes in the gasket and  $Z_i$  is zero for all plaquettes in the gasket except plaquette  $\alpha$ . Upon renormalization according to Eq. (10) the amplitude 1 on one of sites 1,2,3 in plaquette  $\alpha$  will be communicated to sites 1',3',C' in plaquette  $\alpha'$  by  $C^+D$ , see Fig. 1(b). A second renormalization step will communicate the amplitude on sites 1',3',C' in plaquette  $\alpha'$  to sites 1'',3'',C'' in plaquette  $\alpha''$  by  $(C^{(1)})^+D^{(1)}$ , etc. Here  $C^{(1)}$  and  $D^{(1)}$  are the values of the internal-external coupling and of  $D$  appropriate to description of the gasket after one renormalization, from Eq. (8) and (9). Thus to follow the evolution of  $G_{nm}(s)$  at each step of renormalization we need to pay attention only to the amplitudes in the single plaquette to which they are communicated by  $C^+D$  in Eq. (10). To see how this goes we show a particular example in Figs. 2(a) and 2(b). In Fig. 2(a) we show the amplitude at the sites in successive plaquettes for three steps of renormalization at  $s=0.003$  (recall  $s$  sets the time scale). In Fig. 2(b) we show the sum of the amplitude at the three sites in successive plaquettes (for seven steps of renormalization). The labeling employed in this figure is described in the Appendix. From the numbers on Fig. 2(a) or from Fig. 2(b) we see that the sum of the amplitudes in a plaquette is essentially 1.0 until renormalization has carried us to a length scale greater than the average distance to which a particle can move on the time scale on which it is being studied, see the insert in Fig. 2(b). From information like that in Fig. 2(b) we can learn  $\langle x^2 \rangle \propto (Wt)^{2/d_w}$ . We do not pursue that point here.

Instead let us look at the evolution of the amplitudes under renormalization. At  $t=0$  we place amplitude 1 at site  $n$ . This amplitude is spread through the system at each step of renormalization. To calculate  $G_{0n}(t)$  the probability that a particle is at site 0 at time  $t$  given that it was at site  $n$  at time 0, we need to learn the amplitude at site 0. After  $m$  steps of renormalization the amplitude reaches site 0. If when the amplitude reaches site 0 the coupling constants have yet to saturate, then site 0 is importantly connected to its neighbors through  $C$  and the amplitude at site 0 will continue to evolve upon further renormalization. If when the amplitude reaches site 0 the coupling constants have saturated, then site 0 is no longer importantly connected to its neighbors,  $C \rightarrow 0$ , and the

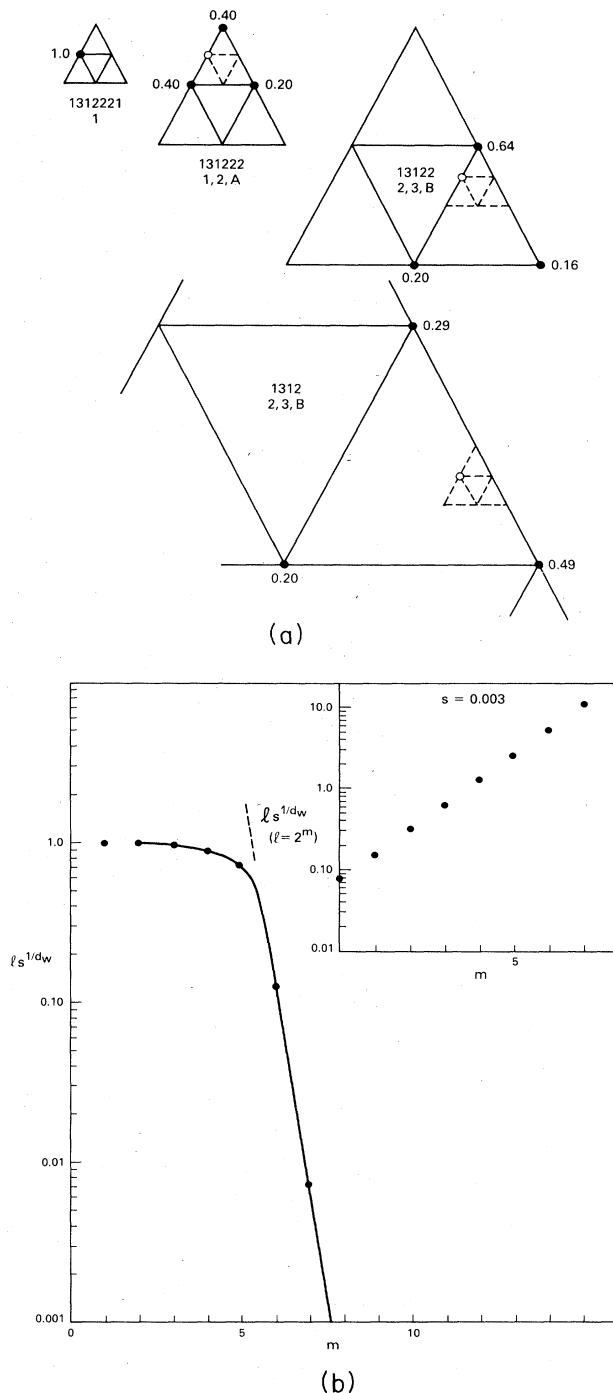


FIG. 2. Evolution of the amplitude. (a) The renormalization procedure communicates the amplitude (at  $t=0$  the particle is at site 1 in plaquette 1312221) to sites in the new plaquette, e.g., to sites 1,3,B in plaquette 131222 after one renormalization. The evolution shown here is for  $s=0.003$ . The sum of the amplitudes is 1.0 until  $l s^{1/d_w} \geq 1$  for plaquette 1312; see the inset of (b) below. (b) The sum of the amplitudes as a function of renormalization for the case shown in (a). After approximately four renormalizations the gasket is being viewed on a length scale  $l \gg s^{-1/d_w}$ ; the sites being examined are no longer readily accessible to the particle. Compare the evolution of the sum and the behavior of  $l s^{1/d_w}$  shown in the insert.

amplitude at site 0 will not evolve further upon continued renormalization. In this latter case we may solve Eq. (7b) in the form

$$G_{0n}(s) = G_{00}(s)Z_{0n}(s), \tag{11}$$

where  $G_{nm}(s) = (s + V^{(\infty)})^{-1}$ . Thus to study  $G_{nm}(s)$  we need only examine the behavior of  $Z_{nm}(s)$  as the LSR procedure for solving Eq. (6) gives the solution in the product form of Eq. (11).

There is a further advantage conferred by the LSR procedure. When the coupling constants have saturated,  $D$  approaches a constant and the further evolution of  $Z$  to sites not yet reached, given by Eq. (10) with  $Z_e = 0$ , depends only upon  $C$ . However,  $C$  evolves as in Eq. (9) and when the coupling constants have saturated this equation has an analytic solution. Thus we are able to derive an analytic expression for the asymptotic behavior of  $Z_{nm}$  and  $G_{nm}(s)$ . We do this below.

Before proceeding we restate some of the background that pertains to the discussion above in a language that may help clarify what has been said. In Fig. 3 we show

the  $l$ - $t$  parameter space for discussion of kinematics; the coordinates are distance  $l$  and time (actually  $s = t^{-1}$ ). The solid curve is at  $\langle l^2 \rangle / a^2 \cong (W/s)^{1/d_w}$ . Region I in Fig. 3 is the region of space readily accessible to a particle on a particular time scale; region II in the figure is the region of space not easily reached by a particle on a particular time scale. The coupling constants that arise in the discussion of the LSR procedure describe various features of particle motion as the motion is viewed on different length scales at fixed time scale i.e., as one moves along the dotted line in the figure. For example, the coupling constant  $C$ , Eqs. (8), (9), and (10), describes the rate at which particles come from a "neighboring" site onto a site to which one is paying attention. Upon renormalization the neighboring sites become more distant,  $C \rightarrow 0$ , and the coupling constant  $V$  approaches a constant.

Equation (7b) becomes easy to solve, etc.<sup>12</sup> Similarly, the amplitudes are communicated intact among sites in region I; they are communicated by  $C$  that is approaching zero in region II. Problems are often easily soluble in region II and a solution there may provide all that is neces-

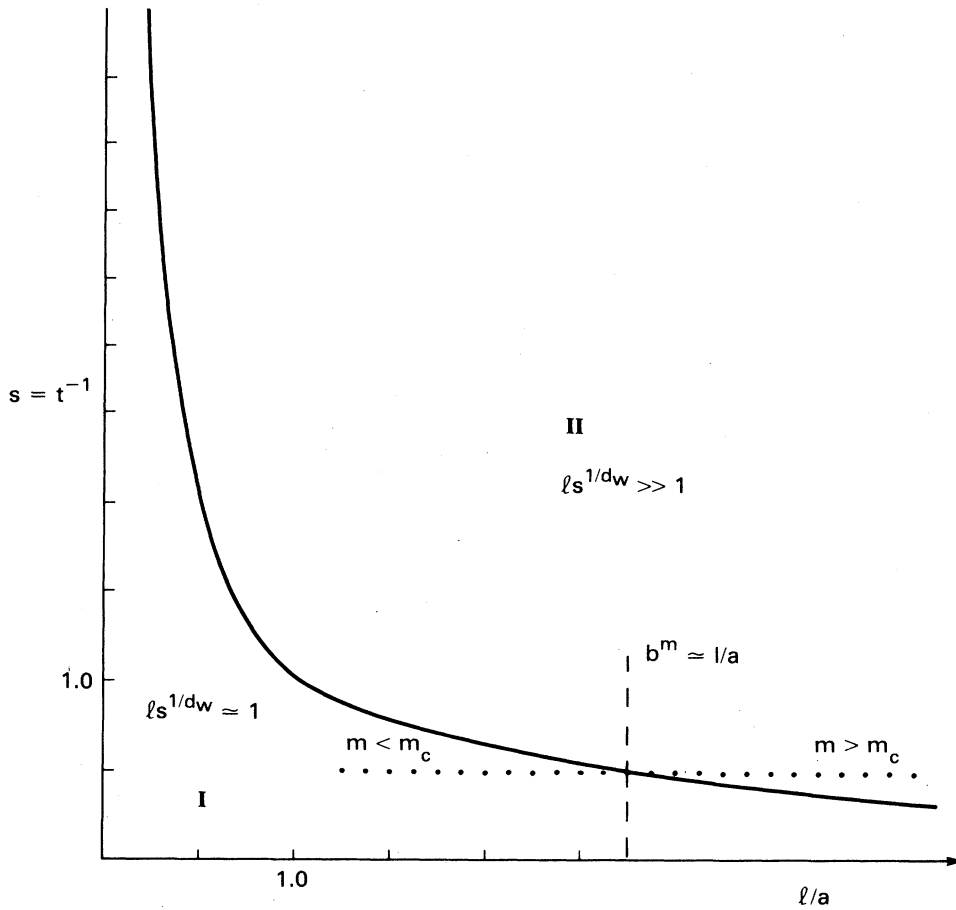


FIG. 3. The distance-time parameter space. The distance-time relation  $(l/a)^2 \cong (Wt)^{1/d_w}$  divides the  $l$ - $t$  space into regions I and II. Points in region I are readily reached on time scale  $t$  ( $t = s^{-1}$ ); points in region II are not readily reached on this time scale. The average behavior of a particle is explored in region I; the asymptotic behavior of a particle is explored in region II. At fixed time scale there is a crossover in length scale that corresponds to a change in the behavior of the coupling constants as renormalization proceeds at  $m_c$  such that  $b^{m_c} \cong l/a \cong (W/s)^{1/d_w}$ .

sary to understand the behavior in region I. After all, to simply learn the location of the transition from region I to region II is to learn a great deal; i.e.,

$$\langle l^2 \rangle / a^2 \cong (Wt)^{2/d_w}, \lim_{t \rightarrow \infty} G_{nn}(t), \dots$$

Finally, a piece of notation: after  $m$  steps of renormalization we look at the system on length scale  $b^m$ . The crossover value of  $m$  is denoted by  $m_c$  where  $ls^{1/d_w} \cong b^{m_c} s^{1/d_w} \cong 1$ ;  $m_c$  depends upon "time",  $s^{-1}$ ; see Fig. 3.

Let us now turn to description of the results of numerical solution to Eqs. (8), (9), and (10). We look briefly at a one dimensional chain, *A*, and in more detail at a Sierpiński gasket, *B*. For both the one-dimensional chain and the Sierpiński gasket (a) we review the results of solution to Eqs. (8) and (9), and (b) we describe the results of solution to Eq. (10).

## A. One dimension

### 1. Iteration of Eqs. (8) and (9)

Iteration of Eqs. (8) and (9) leads to the evolution of the coupling constants that have been described in detail.<sup>12</sup> The essential feature of this evolution is that on a suitable length scale (at fixed time scale)  $C \rightarrow 0$  and  $V$  saturates; i.e., one enters region II in Fig. 3. In region II Eq. (6) can be solved for  $G_{nn}(s)$ ,  $G_{nn}(s) \propto s^{-1/2}$ ;  $G_{nn}(t)$  and  $\langle x^2 \rangle / a^2 \propto Wt$  follow. Solutions to Eqs. (8) and (9) locate the boundary between region I and region II and yield information in various forms that are equivalent to the location of this boundary, i.e.,  $G_{nn}(s)$ ,  $G_{nn}(t)$ ,  $\langle x^2 \rangle / a^2 \propto Wt$ .

### 2. Iteration of Eq. (10)

In Fig. 4 we show  $Z_{0n}(s)$  as a function of  $s$ , from numerical solution to Eq. (10), in the form  $\ln Z_{0n}(s)$  vs

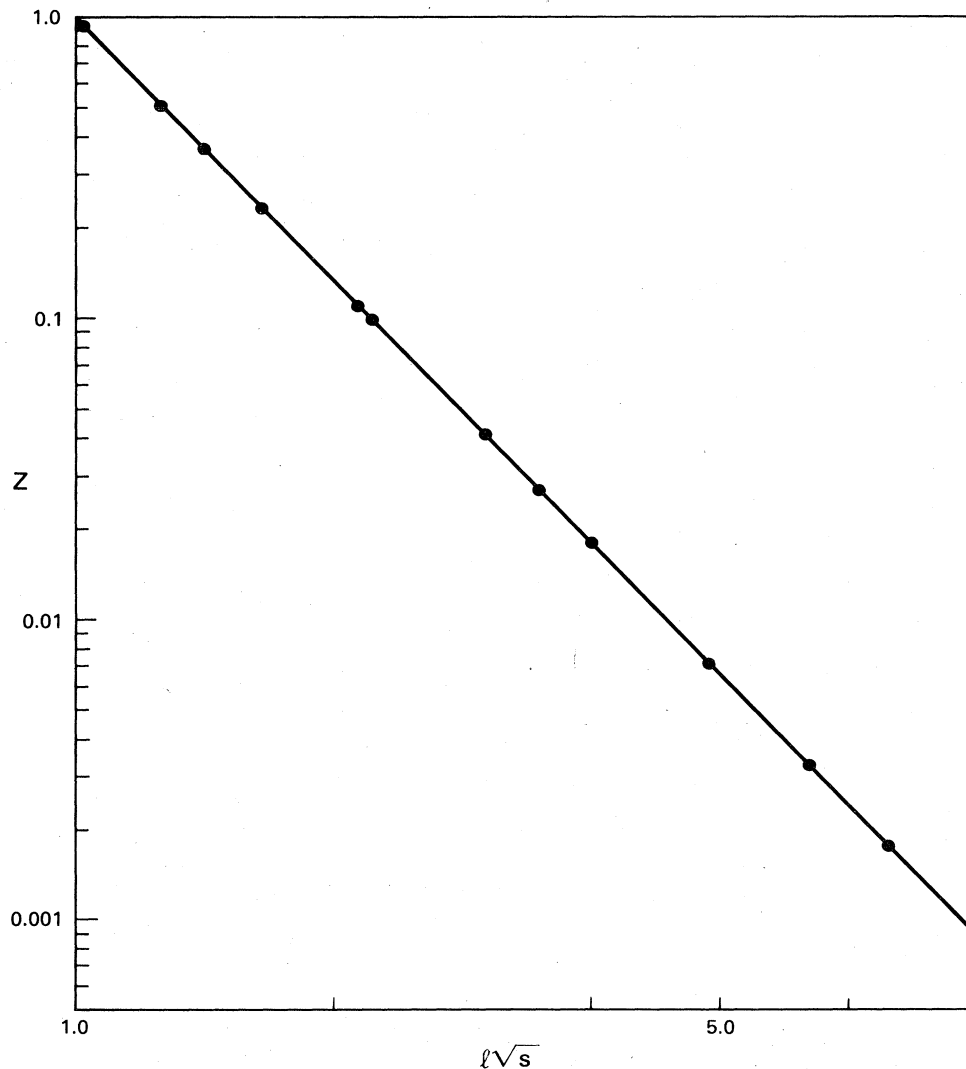


FIG. 4.  $Z$  as a function of distance and time for one dimension. The behavior of  $Z$  as a function of  $l$  and  $s$  is shown by plotting  $\ln Z$  vs  $l/\sqrt{s}$ ; see Eq. (12).

$|l_{0n}| \sqrt{s}$ . Here  $|l_{0n}|$  is the distance from site  $n$  to the origin. From the behavior seen in the figure we may conclude that  $Z_{0n}(s)$  behaves as

$$Z_{0n}(s) = \exp \left[ -\frac{|l_{0n}|}{a} \left( \frac{s}{W} \right)^{1/2} \right]. \quad (12)$$

This result, in agreement with the analytic solution to Eq. (5) for a one-dimensional chain, serves in this case to confirm the numerical procedure and to stimulate an inquiry into the source of the behavior in Eq. (12). The horizontal axis in Fig. 4 involves  $0 \leq |l_{0n}| \sqrt{s} \leq 10$ , i.e., points from both region I and region II of the  $l$ - $t$  parameter space (recall region I and region II are separated from one another at  $|l| \sqrt{s} \cong 1$ ). In Fig. 5 we show the coupling constant  $C$  as a function of  $s$ , from numerical solution to Eqs. (8) and (9), in the form  $\ln(C/\sqrt{s})$  vs  $|l_{0n}| \sqrt{s}$ . From the behavior seen in the figure we may conclude that

$$C_{0n} \sim \sqrt{s} \exp \left[ -\frac{|l_{0n}|}{a} \left( \frac{s}{W} \right)^{1/2} \right] \quad (13)$$

for  $|l_{0n}| \sqrt{s}$  in region II. [The evolution of  $C$  in region I is well known and different from that in Eq. (13).] The

evolution of the amplitudes to greater and greater distances (region II) is given by Eq. (10) with  $D=(s+V)^{-1}$  a constant,  $Z_e=0$ , i.e., by the evolution of  $C$ . Thus from the behavior of  $C$  in Fig. 5 we understand the behavior of  $Z$  in Fig. 4. How does the behavior of  $C$  in region II come about? An analytic answer to this question is provided by Eq. (9). In region II  $V$  and  $D$  have reached constant value,  $V^{(\infty)} \cong \sqrt{s}$ ,  $D \cong V^{(\infty)^{-1}}$ , Eq. (9) has the form

$$C^{(m+1)} = \frac{1}{V^{(\infty)}} (C^{(m)})^2, \quad (14)$$

with  $C^{(m)}$  we denote the value of  $C$  after  $m$  iterations of Eqs. (8) and (9). Seeking a solution to Eq. (14) in the form  $C^{(m)} = \sqrt{s} \exp(-ab^m \sqrt{s})$  leads to  $b=2$ . The form of  $C$  in Eq. (13) and of  $Z$  in Eq. (12) follow upon writing  $|l_{0n}| = ab^m$ .

We may summarize the results for the solution to Eqs. (8), (9), and (10) in terms of statements about the scaling of the coupling constants. For fixed  $s$  and  $m_c(s)$  such that  $b^{m_c(s)} s^{1/d_w} \cong 1$ ;

$$\begin{aligned} m &\lesssim m_c; & V^{(m+1)} &\cong b^{-w} V^{(m)}, \\ m &\gtrsim m_c; & W^{(m+1)} &\cong b^{-w} W^{(m)}, \end{aligned} \quad (15)$$

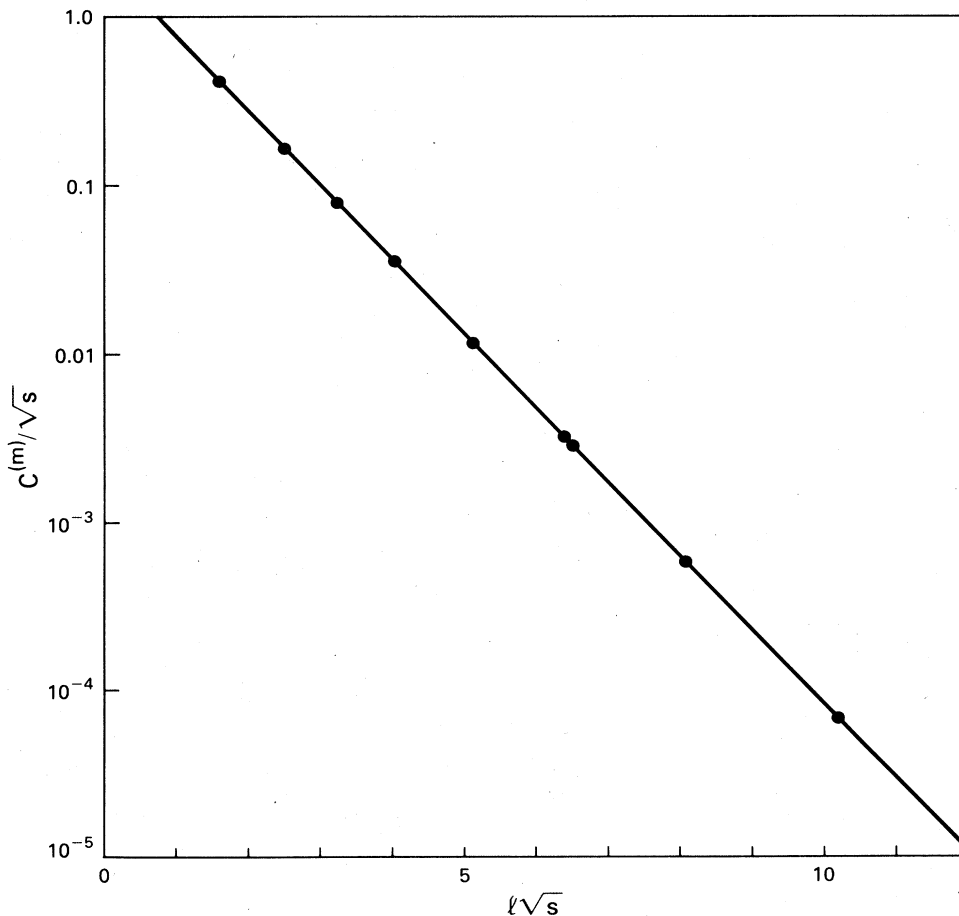


FIG. 5. Behavior of the coupling constants. The behavior of the coupling constants,  $C$ , as a function of distance,  $l$ , and time scale is shown by plotting  $\ln(Z/\sqrt{s})$  vs  $l\sqrt{s}$ . Here  $l$  is the distance between the sites coupled by  $C$  after renormalization. See the discussion below Eq. (12) that relates the behavior of  $Z$  to the behavior of  $C$ .

$$m \geq m_c; V^{(m)} \cong V^{(m_c)} \propto s^{1/d_w}, \tag{16}$$

$$W^{(m)} \sim W^{(m_c)} \exp(-b^{m-m_c}),$$

$W^{(m_c)} \cong V^{(m_c)} \cong b^{-m_c} \cong s^{1/d_w}$ . These scaling relations are written in a form more general than the one-dimensional problem that gave rise to them.

**B. Sierpiński gasket**

*1. Iteration of Eqs. (8) and (9)*

Iteration of Eqs. (8) and (9) for the Sierpiński gasket leads to evolution of the coupling constants that has been described in detail.<sup>6,7</sup> The remarks in subsection A 1 apply equally to the results found in Ref. 6. In addition, for the Sierpiński gaskets, examination of the behavior of the scaling of the coupling constants leads to the scaling relation, Eq. (2) and the Einstein relation, Eq. (3).

*2. Iteration of Eq. (10)*

In Fig. 6 we show  $Z_{0n}(s)$  as a function of  $s$ , from numerical solution to Eq. (10), in the form  $\ln Z_{0n}(s)$  vs  $|l_{0n}^{(T)}| s^{1/d_w}$  for several values of  $s$ . We note immediately in contrast to Fig. 4, which shows  $Z_{0n}$  as a function of  $s$  for one dimension, that while the average features of  $Z_{0n}$  appear to be captured reliably by  $\exp(-|l|s^{1/d_w})$ , Fig. 6 shows evidence for, fluctuations about this average behavior. The evidence in Fig. 6 is even more surprising than at first sight because the distance  $l_{0n}^{(T)}$  used in plotting points on the horizontal axis is not Euclidean distance

$$l^{(E)} = |\mathbf{x}_n - \mathbf{x}_0|, \tag{17}$$

where  $\mathbf{x}_n$  locates site  $n$  and  $\mathbf{x}_0$  locates site 0. It is the distance  $l^{(T)}$ , which might be termed the "lacunar distance," calculated as follows. Consider two sites  $n$  and  $m$  on pla-

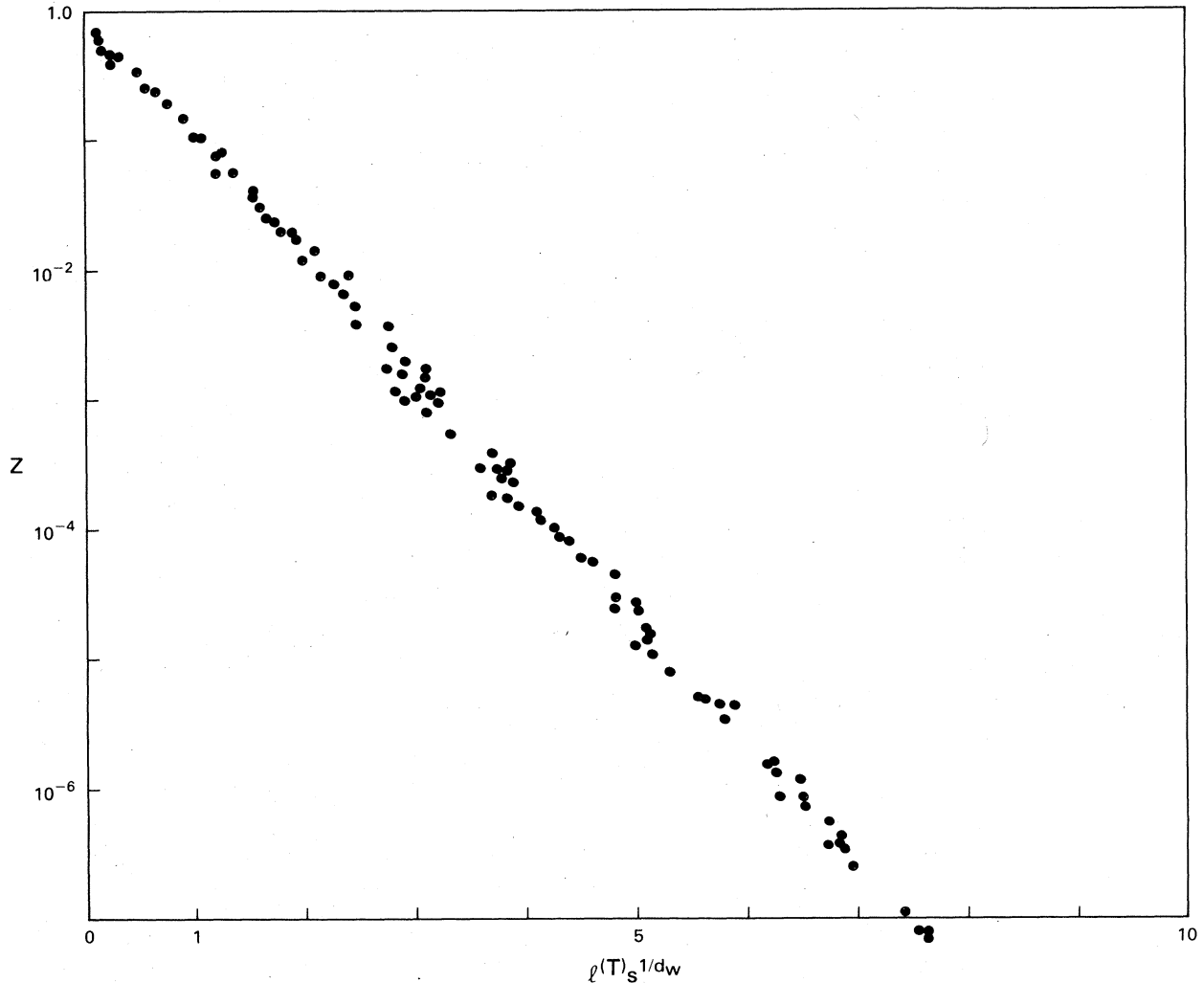


FIG. 6.  $Z$  as a function of distance and time for a Sierpiński gasket. The behavior of  $Z$  as a function of  $l$  and  $s$  is shown by plotting  $\ln Z$  vs  $l s^{1/d_w}$ ; see Eq. (19). The distance  $l$  used in this plot is the lacunar distance defined in Eq. (18) and illustrated in Fig. 7. The fluctuations in  $Z_{nm}(s)$  that occur at a given value of  $l s^{1/d_w}$  are due in part to pairs of points at the same relative distance (thus the same value of  $l$ ) that reside in different environments on the gasket.

quettes  $\alpha$  and  $\beta$ , respectively. Take these plaquettes to have coordinates  $X_1, X_2, \dots, X_7$  and  $Y_1, Y_2, \dots, Y_7$ . The coordinates  $X_1, \dots$  have values 1, 2, and 3 for a Sierpiński gasket. A general coordinate is denoted by  $X_l$  or  $Y_l$ . If a coordinate  $X_l$  of site  $n$  differs from coordinate  $Y_l$  of site  $m$ , then there is a "lake" of size  $2^l$  between site  $n$  and site  $m$ . For  $l^{(T)}$  we take

$$l^{(T)} = \sum_{l=1}^7 2^l \Delta_l, \tag{18}$$

where  $\Delta_l$  is one if  $X_l$  is different from  $Y_l$  and zero otherwise. This definition is illustrated in Fig. 7. In Fig. 8 we show  $(-\ln Z_{0n})/(ls^{1/d_w})$  vs  $ls^{1/d_w}$  for  $l$  the Euclidean distance from Eq. (17) (lower curve) and the lacunar distance from Eq. (18) (upper curve). From Fig. 8 we see that, for  $ls^{1/d_w} \gg 1$ ,  $Z_{0n}$  fluctuates less when  $l$  is the lacunar distance whereas, for  $ls^{1/d_w} \approx 1$ ,  $Z_{0n}$  fluctuates less when  $l$  is the Euclidean distance.

Let us first deal with the average properties of  $Z_{0n}$ . From Fig. 6 we see that on average  $Z_{0n}(s)$  is given by

$$Z_{0n}(s) = \exp \left[ -\alpha \frac{|l_{0n}^{(T)}|}{a} \left( \frac{s}{w} \right)^{1/d_w} \right], \tag{19}$$

where  $\alpha \cong 2.15$  from Fig. 6 (and Fig. 8). This result is understood by an argument similar to that above for Eq. (12) in terms of the behavior of  $C$ . We find, from a numerical study of Eqs. (8) and (9) beyond the point at which the recursion relations saturate, that  $C_{0n}$  behaves as  $\exp(-|l_{0n}|s^{1/d_w})$  in analogy to Eq. (13) and that the argument for this behavior based on Eq. (14) is confirmed. We do not show these numerical results. [The scaling behavior of the coupling constants given by Eqs. (15) and (16), confirmed in these studies, gives rise to a correct description of the average behavior of  $Z_{nm}(s)$ ,  $G_{nm}(s)$ .]

It is clear from Fig. 6 that the average behavior of  $Z_{0n}$  given by Eq. (19) with  $l^{(E)}$  or  $l^{(T)}$  is modified by a factor,

$$Z(\mathbf{x}, \mathbf{x}'; s) = F(\mathbf{x}, \mathbf{x}') z(|\mathbf{x} - \mathbf{x}'| s^{1/d_w}), \tag{20}$$

$F$  which depends on  $\mathbf{x}$  and  $\mathbf{x}'$ , Fig. 8. The source of this factor is the detailed structure of the fractal. The envi-

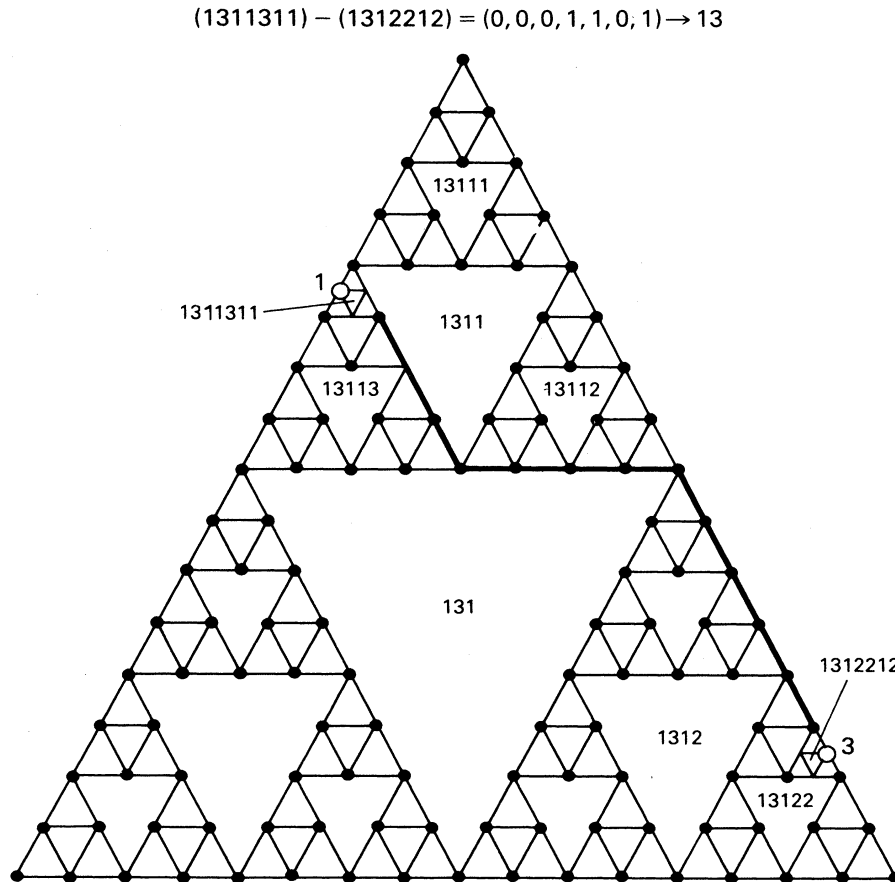


FIG. 7. Lacunar distance. The lacunar distance defined in Eq. (18) is illustrated. This distance is very nearly the distance along the shortest path from 1 to 3 shown as a solid black line.

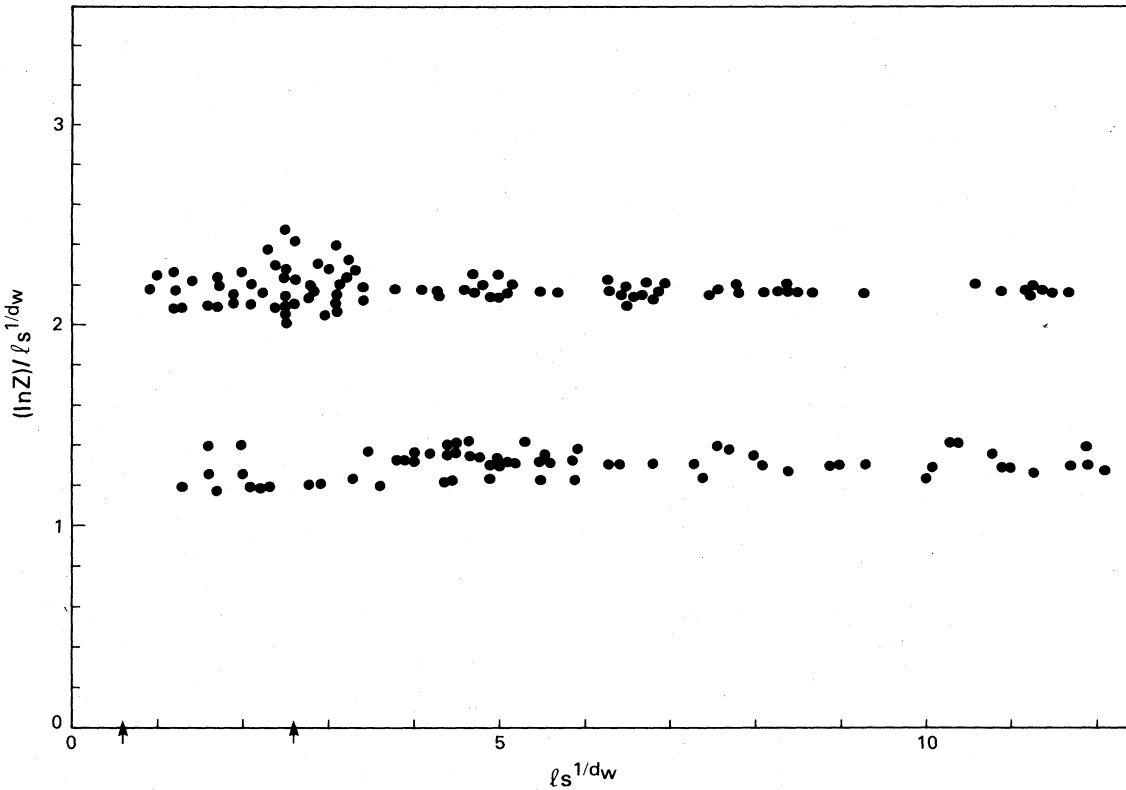


FIG. 8. Behavior of  $F_{nm}(s)$ . The function  $F_{nm}(s)$  that describes fluctuations in the behavior of  $Z_{nm}(s)$  about the average behavior, given by Eq. (19), is plotted as a function of  $l s^{1/d_w}$  for the lacunar (upper curve) and Euclidean (lower curve) definitions of distance.

ronment through which a particle propagates in going distance  $|\mathbf{x}-\mathbf{x}'|$  is a function of  $\mathbf{x}$  and  $\mathbf{x}'$ . On the other hand, it is not a strong function of  $\mathbf{x}$  and  $\mathbf{x}'$  for certainly the fluctuations around the average behavior are relatively mild. This is particularly true for  $l s^{1/d_w} \gg 1$  if  $l$  is the lacunar distance. Or from the evidence in Fig. 8 for  $l s^{1/d_w} \geq 3$ . Distance  $l$  such that  $l s^{1/d_w} \gg 3$  are in region II (Fig. 3) and are distances that a particle cannot easily reach on time scale  $s^{-1}$ . To reach these distances a particle must use the most direct path. The length of this path is essentially the lacunar distance defined in Eq. (18). For  $l s^{1/d_w} \approx 1$  the Euclidean distance is superior to the lacunar distance as we would expect.

### III. DISCUSSION

Let us begin discussion of the results reported above by summarizing them. For the Sierpiński gasket we find the off-diagonal conditional probability for  $l s^{1/d_w} \geq 1$  to be of the form

$$G_{nm}(s) = G_{nn}(s) Z_{nm}(s) \tag{21}$$

with

$$Z_{nm}(s) = F_{nm}(s) z(|l_{nm}| s^{1/d_w}), \tag{22}$$

where  $|l_{nm}|$  is a measure of the distance between site  $n$

and site  $m$  and

$$z(x) = \exp(-\alpha x). \tag{23}$$

(a) The constant  $\alpha$  and  $F_{nm}(s)$  are functions of the choice of the measure of  $|l_{nm}|$ .

(b) The fluctuations about the average behavior in  $z(x)$  are relatively mild.

(c) The result in Eqs. (21)–(23) can be understood in terms of the scaling properties of the coupling constants, Eqs. (15) and (16), implied by the recursion relations, Eqs. (8)–(10).

(d) Further details of the content of Eqs. (21)–(23) are reported in Sec. II.

For the remainder of this discussion we set  $F_{nm}(s) = 1.0$  and take  $G(\mathbf{x}, \mathbf{x}'; s)$  to be approximated by a function of  $\mathbf{r} = \mathbf{x} - \mathbf{x}'$  in the form

$$G(\mathbf{r}, s) = G(0, s) \exp \left[ -\alpha \frac{|\mathbf{r}|}{a} \left( \frac{s}{W} \right)^{1/d_w} \right], \tag{24}$$

where

$$G(0, s) = \frac{1}{W} \left( \frac{W}{s} \right)^k \text{ and } k = 1 - d_F/d_w.$$

We cannot construct an exact inverse Laplace transform of Eq. (24). However, from the pieces

$$L^{-1}G(0,s) \rightarrow \frac{1}{(Wt)^{d_F/d_w}} \tag{25}$$

and

$$L^{-1} \exp \left[ -\alpha \frac{|\mathbf{r}|}{a} \left( \frac{s}{W} \right)^{1/d_w} \right] \rightarrow \exp \left[ -\alpha \left( \frac{|\mathbf{r}|}{a} \frac{1}{(Wt)^{1/d_w}} \right)^\nu \right], \tag{26}$$

where  $\nu = d_w(d_w - 1)^{-1}$  [Eq. (26) can be found from looking at the stationary point of the argument in the formal definition of the inverse transform or by going from the right-hand side to the left-hand side] we infer ( $\beta$  is a constant of order 1)

$$G(\mathbf{r};t) = A \frac{1}{(Wt)^{d_F/d_w}} \exp \left[ -\beta \left( \frac{|\mathbf{r}|}{a} \frac{1}{(Wt)^{1/d_w}} \right)^\nu \right]. \tag{27}$$

We fix the constant  $A$  using

$$\int d\mathbf{r} \rho(\mathbf{r}) G(\mathbf{r};t) = 1 \tag{28}$$

with  $\rho(\mathbf{r}) \cong |\mathbf{r}|^{d_F-d}$ . That is from the requirement

$$\int d|\mathbf{r}| |\mathbf{r}|^{d_F-1} G(\mathbf{r};t) = A \int du u^{d_F-1} \exp(-\beta u^\nu) = 1.$$

We use Eq. (28) to calculate  $\langle |\mathbf{r}|^2 \rangle$ ;

$$\langle |\mathbf{r}|^2 \rangle = \int d\mathbf{r} \rho(\mathbf{r}) |\mathbf{r}|^2 G(\mathbf{r};t) \propto (Wt)^{2/d_w} \tag{29}$$

and find the distance-time relationship that we want. Finally we note that Eq. (27) for  $G(\mathbf{r};t)$  agrees with the result found by Fisher<sup>10</sup> in discussion of a somewhat related problem. (See also Angels d'Auriac *et al.*<sup>14</sup> and Cloiseaux.<sup>15</sup>)

While Eq. (27) for  $G(\mathbf{r};t)$  is in agreement with the result of Fisher and yields  $\langle |\mathbf{r}|^2 \rangle \propto (Wt)^{2/d_w}$ , it does not

satisfy the Chapman-Kolmogorov equation (CK), i.e.,

$$\int dy \rho(\mathbf{y}) G(\mathbf{x}-\mathbf{y};\tau) G(\mathbf{y}-\mathbf{x}';t-\tau) = G(\mathbf{x}-\mathbf{x}';t). \tag{30}$$

Banavar and Willemsen<sup>11</sup> have used this equation to test the validity of the proposed form

$$G_{BW}(\mathbf{r};t) = \frac{A}{(Wt)^{d_F/d_w}} \exp \left[ -\frac{|\mathbf{r}|^{d_w}}{Wt} \right] \tag{31}$$

and find quite good results. As above we fix  $A$  in Eq. (31) using

$$\int d\mathbf{r} \rho(\mathbf{r}) G(\mathbf{r};t) = A \int du u^{d_F-1} \exp(-u^{d_w}) = 1$$

and find  $\langle |\mathbf{r}|^2 \rangle \cong (Wt)^{2/d_w}$ . Just what one would like.

The relationship of Eq. (27) to Eq. (31) is understood with reference to Fig. 3. Equation (24) and Eq. (27) which are based on it are valid in region II of  $l-t$  space. The CK equation, involving  $[G(\mathbf{r};t)]^2$ , is sensitive to the behavior of  $|\mathbf{r}|$  and  $t$  in region I of  $l-t$  space. For example the integral [Eq. (30) at  $\tau=t/2$ ]

$$\int d\mathbf{r} \rho(\mathbf{r}) [G(\mathbf{r};t/2)]^2 \propto \int d|\mathbf{r}| |\mathbf{r}|^{d_F-1} \times \exp \left[ -2 \left( \frac{|\mathbf{r}|}{t^{1/d_w}} \right)^\nu \right] \tag{32}$$

gets maximum contribution from

$$\frac{|\mathbf{r}|}{t^{1/d_w}} \cong 0.5,$$

in region I of  $l-t$  space. In Fig. 9 we show the region of  $l-t$  space probed in normalization of  $G(\mathbf{r};t)$ , in application of the CK equation ( $\tau=t/2$ ) and in calculation of  $\langle |\mathbf{r}|^2 \rangle$ . Equations (27) and (31) describe the conditional probability in essentially disjoint regions of  $l-t$  space. With Eqs. (27) and (31) we have a reasonable description of the leading behavior of  $G(\mathbf{r};t)$  in all of space. We have

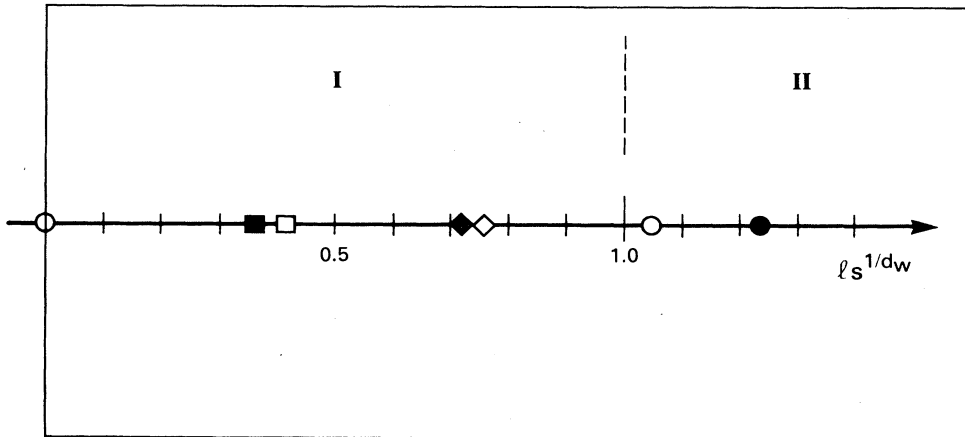


FIG. 9. Location of calculations in  $l-t$  space. Calculations of the norm, Eq. (28),  $\langle |\mathbf{r}|^2 \rangle$ , Eq. (29) and the CK equation, Eq. (30), probe the description of particle motion in different regions of  $l-t$  space. This is illustrated here for the function  $G(\mathbf{r};t)$  from Eq. (27), closed symbols, and for the function  $G(\mathbf{r};t)$  from Eq. (31), open symbols.

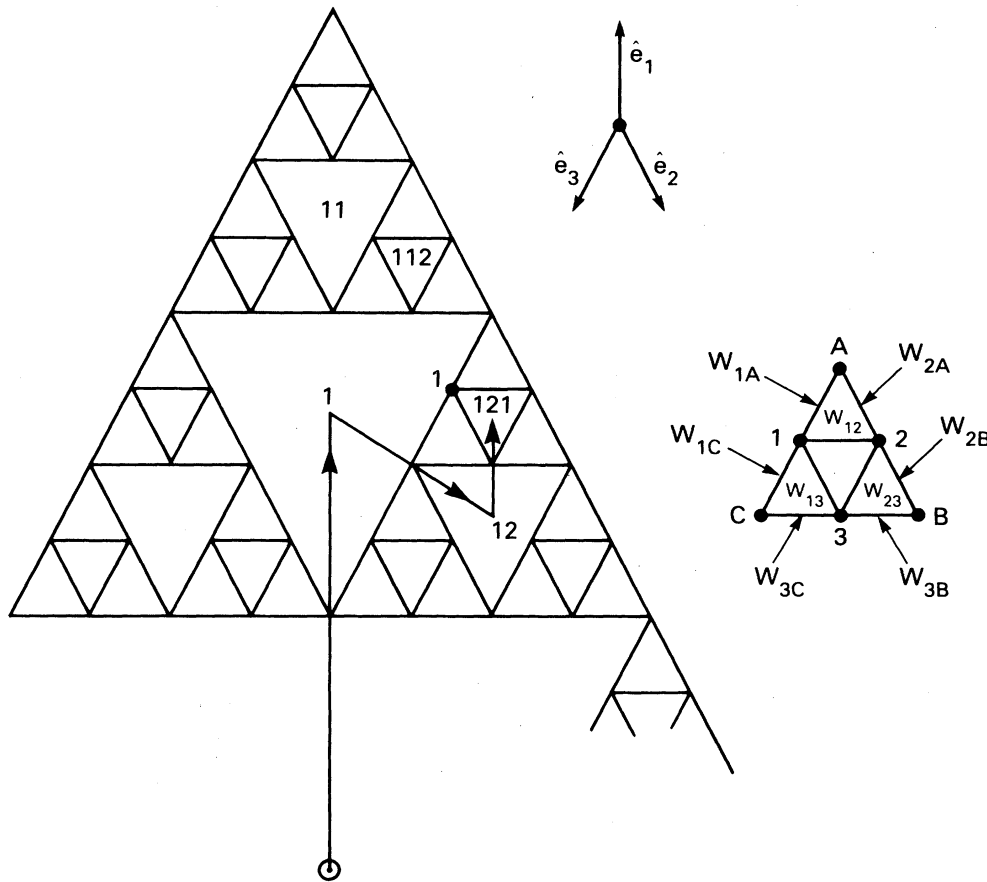


FIG. 10. Plaquette location. Plaquettes are denoted by components 1,2,3 that denote the unit vector involved, i.e.,  $\hat{e}_1, \hat{e}_2, \hat{e}_3$ . Sites associated with a plaquette are 123 (internal sites) and ABC (external sites).

no satisfactory understanding of the fluctuations about this average behavior.

*Note added in proof.* Since this paper was submitted for publication, a paper by O'Shaughnessy and Procaccia on the same subject has been published in Phys. Rev. Lett. 54, 455 (1985).

ACKNOWLEDGMENTS

The author has benefited from extensive discussions with J. Banavar and Jorge Willemsen.

APPENDIX

Notation for finding sites on the gasket. The gasket has sites as in the example in Fig. 10 located with a vector notation that uses the unit vectors

$$\hat{e}_1 = (0, 1),$$

$$\hat{e}_2 = \left[ \frac{1}{2}, \frac{-\sqrt{3}}{2} \right],$$

and

$$\hat{e}_3 = \left[ \frac{-1}{2}, \frac{-\sqrt{3}}{2} \right].$$

The plaquette found at the tip end of the vector  $\mathbf{x}_{121} = 4\hat{e}_1 + 2\hat{e}_2 + \hat{e}_3$  is denoted 121. The sites reached from each plaquette are 1, 2, and 3 for the interior sites and A, B, and C for the exterior sites as shown in the figure. The 2187 plaquettes used in the numerical work,  $2187 = 3^7$ , are denoted by 7-component vectors, e.g.,  $\mathbf{X} = 1233131, X_7 = 1, X_6 = 2, X_5 = 3, \dots, X_1 = 1$  or

$$\mathbf{X} = 2^6\hat{e}_1 + 2^5\hat{e}_2 + 2^4\hat{e}_3 + 2^3\hat{e}_3 + 2^2\hat{e}_1 + 2^1\hat{e}_3 + 2^0\hat{e}_1.$$

After one renormalization a 6-component vector suffices to locate the  $3^6 = 729$  remaining plaquettes; these vectors are denoted

$$\mathbf{X}^{(1)} = 4123313 = 2^6\hat{e}_1 + 2^5\hat{e}_2 + 2^4\hat{e}_3 + 2^3\hat{e}_3 + 2^2\hat{e}_1 + 2^1\hat{e}_3.$$

The plaquette 1233131 evolves upon renormalization, 4123313, 4412331, 4441233, ... . With this notation it is straightforward to assign nine different bonds to each plaquette and to keep track of the set of bonds that describe the system after each renormalization, etc.

- <sup>1</sup>B. B. Mandelbrot, *The Fractal Geometry of Nature* (Freeman, San Francisco, 1982).
- <sup>2</sup>S. Alexander and R. Orbach, *J. Phys. Lett. (Paris)* **43**, L625 (1982).
- <sup>3</sup>R. Rammal and G. Toulouse, *J. Phys. Lett. (Paris)* **44**, L13 (1983).
- <sup>4</sup>Y. Gefen, A. Aharony, and S. Alexander, *Phys. Rev. Lett.* **50**, 77 (1983).
- <sup>5</sup>Y. Gefen, A. Aharony, B. B. Mandelbrot, and S. Kirkpatrick, *Phys. Rev. Lett.* **47**, 1771 (1981).
- <sup>6</sup>R. A. Guyer, *Phys. Rev. A* **29**, 2751 (1984), see also Ref. 2.
- <sup>7</sup>R. A. Guyer, *Phys. Rev. A* **30**, 1112 (1984); T. Vicsek, *J. Phys. A* **16**, L647 (1983).
- <sup>8</sup>F. Leyvraz and H. E. Stanley, *Phys. Rev. Lett.* **51**, 2048 (1983).
- <sup>9</sup>We go back and forth between discrete and continuous notation,  $(n, m) \leftrightarrow (x, x')$ . The continuum has density  $\rho(x) \cong |x|^{d_F-d}$ , see Sec. III. We take the coupling constant  $W$  and the length  $a$  to characterize the discrete form of the diffusion equation. These parameters are explicitly exhibited on occasion when dimensionless quantities are useful.
- <sup>10</sup>M. E. Fisher, *J. Chem. Phys.* **44**, 616 (1966).
- <sup>11</sup>J. R. Banavar and J. F. Willemsen, *Phys. Rev. B* **30**, 6778 (1984).
- <sup>12</sup>R. A. Guyer, *Phys. Rev. A* **29**, 2114 (1984).
- <sup>13</sup>J. V. José, *J. Phys. A* **16**, L205 (1983).
- <sup>14</sup>J. C. Angles d'Auriac, A. Benoit, and R. Rammal, *J. Phys. A* **16**, 4039 (1983).
- <sup>15</sup>J. des Cloizeaux, in *Phase Transitions; Carègese 1980*, edited by M. Levy, J. C. Le Guillou, and J. Zinn-Justin (Plenum, New York, 1982), pp. 371–394.